Prediction of Material Removal Rate in Die-Sinking Electrical Discharge Machining

Nur Sheril Loke Binti Izwan, Zhujian Feng, Jigar Bimal Patel, and Wayne Nguyen Hung[*]

Texas A&M University, College Station, Texas, USA.
Sherilaini@tamu.edu, Fengzhujian@tamu.edu, Jpatel22@tamu.edu, Hung@tamu.edu

Abstract

This paper proposes a semi-empirical model to predict material removal rate in die-sinking electrical discharging machining (EDM). Four different workpiece materials -- high strength steel, high strength low alloy steel, brass, and aluminum -- are utilized in the study. Full factorial experiments using peak current, on-time at two levels are selected for each workpiece material while keeping other parameters the same. The removed volumes are calculated by measuring sectional area of an EDM'ed hole and its dimensions. The developed MRR model includes the EDM cumulative electrical charge for each cycle and melting temperature of workpiece material; it predicts two orders of magnitude closer to experimental data compared to a published model that is based on melting temperature and peak current alone.

Keywords: Electrical Discharge Machining, Nontraditional Machining, Material Removal Rate, Microstructure

1 Introduction

Electrical discharge machining (EDM) is a nontraditional technique that can remove any conductive material through a series of electrical sparks. The acceleration of ions and electrons, ionized from an inter-electrode medium, impacts on both electrode and workpiece surfaces. Such impact generates local heat that melts the material as evidenced from remaining craters with minute blobs of molten materials. Die sinking EDM uses an electrode to plunge into a workpiece and create the negative shape of the electrode, while wire-EDM utilizes uniform wire that moves continuously and gradually cuts through a workpiece. Although EDM was invented in 1940s and has been developed commercially, most published documents present results for specific cases, i.e., experimental EDM results for specific materials at certain operating conditions. The objective of this research is to develop a general semi-empirical model to predict material removal rate in die-sinking EDM.

---

[*] Corresponding author.

2 Literature Review

Current (A)

ab: peak current I_p
ad: on-time t_{on}
de: off-time t_{off}
ae: cycle T
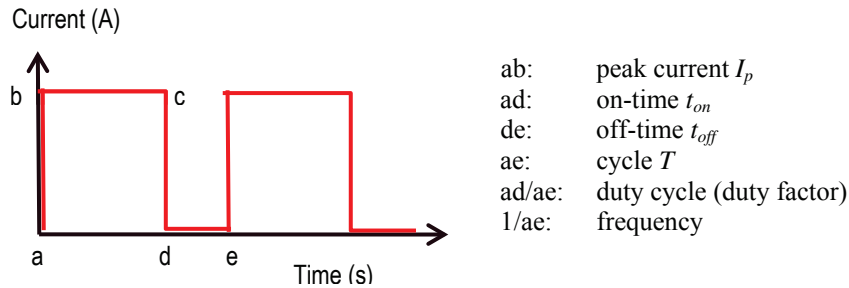ad/ae: duty cycle (duty factor)
1/ae: frequency

Figure 1: Pulsed current in EDM

A pulsed current is traditionally used in EDM. Figure 1 shows the theoretical pulsed current that flows across the electrodes. A bank of external capacitors is charged then electrically discharged during the on-time to generate simultaneous sparks that remove discrete amount of materials as debris. Such debris is then flushed away during the off-time to reveal a fresh workpiece surface for the next spark eroding cycle. Assuming a constant peak current, the area under the current-time plot is:

$$A = \int_0^T I(t)dt = \int_0^{t_{on}} I(t)dt = I_p t_{on} \tag{1}$$

This area *A*, therefore, is the cumulative charge *Q* that would be discharged to generate a spark. Most researchers consider peak current and on-time separately rather than combining them when studying the workpiece material removal rate (MRR).

Ojha et al. (2010) wrote a comprehensive review of how MRR can be enhanced. The paper concluded that MRR improved with a higher gap voltage, peak current, and on-time. The off-time also weakly contributed to MRR since debris must be adequately flushed by a suitable method with optimal dielectric fluid.
Singh et al. (2012) machined D3 tool steel by die-sinking EDM with either copper or brass electrodes in kerosene dielectric. They found that a copper produced MRR at three times more than that when using an equivalent brass electrode. The on-time contributed to higher MRR significantly, but off-time had a less drastic change in MRR. A linearly dependence of MRR to both on-time and peak current was established by Singh and Garg (2009) when wire-EDM H11 tool steel. Increasing the off-time, however, decreased the MRR perhaps due to wasting time after effectively flushing debris generated during the sparking period. Goswami and Kumar (2014) wire-EDM'ed Ninomic alloy. The authors varied on-time, off-time, gap voltage, peak current, wire feed and wire tension in their experiments and concluded that MRR depended not only on the on-time t_{on} and off-time t_{off}, but also the products $(t_{on * } t_{off})$ and $(t_{on * } I_p)$. Shabgard et al. (2011) studied die-sinking EDM of H13 tool steel using copper electrode. Longer on-time and peak current increased MRR but also increased the white recast layer and heat affected zone.

The MRR for EDM was documented to be proportional to the peak current but not the shape of the current-time profile, i.e., the model is independent to both on-time and off-time (Weller, 1984):

$$MRR = \frac{664\,I_p}{T_m{}^{1.23}} \tag{2}$$

Where MMR: material removal rate (mm^3/s)
        I_p: peak current (A)
        T_m: workpiece melting temperature (°C)

Bobbili et al. (2015) studied the MMR of 7017 aluminum and armor steel by wire-EDM. The effect of peak current was embedded in the input power. The authors applied the Buckingham Pi theorem and found that MRR depended on both process parameters and the workpiece thermal properties. The MRR depended on on-time but not directly proportional to the current:

$$MRR = A_1\left(T_{on}^{1/2}\alpha^{3/2}\right)\left(\alpha^{3/2}T_{on}^{1/2}\,FP\,E^{-1}\right)^{B1}\left(T_{on}\,HV\,\alpha^{-1}\right)^{C1} \tag{3}$$

Where FP: flushing pressure
MMR: material removal rate E: power
A_1, B_1, C_1: constants HV: latent heat of workpiece material
T_{on}:   on-time α: thermal diffusivity of workpiece material

Dave et al. (2012) studied the orbital EDM on Inconel 718 and copper electrode. For this specific case, the MRR model was derived by Taguchi experimental method to be:

$$MRR = 0.549\frac{I^{0.885}V^{0.203}t_{on}^{0.058}DF^{0.335}}{R_o^{0.479}S_o^{0.103}} \tag{4}$$

Equation (4) predicts that MRR would increase with both current and on-time. The same authors later used Pi theorem to derive another MRR model for the same conditions.

$$MRR = 0.7711\frac{I^{0.955}t_{on}^{0.109}}{R_o^{0.542}S_o^{0.0625}} \tag{5}$$

Where
MMR: material removal rate DF: duty factor
I: current R_o: orbiting radius
V: gap voltage S_o: orbiting speed
t_{on}:   on-time

Miller et al. (2004) used wire-EDM to cut porous metal foams, metal bond porous metal foams, metal bond diamond grinding wheels, sintered Nd-Fe-B magnets, and carbon–carbon bipolar plates. The MRR maps against sparking cycle were developed to show an effective process bounded by wire breaking at low sparking cycle and electric short at high sparking cycle. The region was also bounded by the ranges of on-time where higher on-time contributed to larger MRR. Higher MRR was observed when wire-EDM material with low melting temperature and low electrical resistivity.

Sultan et al. (2014) published their study of die sinking EDM using copper tube electrode on EN353 steel workpiece. Box-Behnken design was used for planning and executing main experimentation with on-time, off-time, and peak current as the input parameters. The MRR was reported to be dependent not only on both peak current and on-time, but also off-time:

$$MRR = 20.12185 + 0.015014\,t_{on} - 0.23106\,t_{off} - 0.42890\,I_p + 2.88377 \times 10^{-5}\,t_{on}^2 + 4.52138 \times 10^{-3}\,I_p^2 - 8.47222 \times 10^{-4}\left(t_{on}t_{off}\right) + 0.013052\left(t_{off}I_p\right) \tag{6}$$

Using artificial neural network technique, Yahya et al. (2011) investigated the MRR of steel using copper electrode and BP200 mineral oil as dielectric fluid. The main input variables were on-

time, off-time, sparking frequency, and peak current. At on-time around 50 µs, the MRR increased 3 times from 18 to 55 mm^3/min when the peak current increased approximately the same ratio from 4A to 12.5A.

3 Experiments

Metallic alloys with different melting temperatures were selected. The 6061-T6 aluminum, high strength low alloy steel Domex 550MC, and brass alloy CA 360 were machined to plates of approximately 50 x 70 mm and thickness between 3-8 mm. The high strength low alloy (HSLA) steel was also included to compare its machinability against the Domex steel. The Sodick K1C die-sinking EDM was used to form holes with a rotating and hollow copper electrode (ø2 mm outside diameter and ø0.8 mm inside diameter) (Figure 2). The constant electrode rotation speeds were measured four times by clocking the required times for 20 rotations to be 123, 119, 122, and 122 rpm. The peak current was set at 13A and 35A, while on-time was set at 20µs and 28µs at 50% duty cycle, this meant both the on-time and off-time were the same. Other parameters were kept constants: 8 volt servo voltage regulator, 0.22 µF capacitor, Vitol-KS dielectric fluid (900 Ωcm resistivity, 0.925 m^2/s kinematic viscosity) for through electrode flushing. Machining times (15 s for thin plates and 18 s for thicker plates) were measured with a stop watch; the clock started when the gap voltage experienced a significant drop as observed on an analog voltage gage. The sudden changes also coincided with the first sparking sound when the electrode approaching a workpiece. Each sample surface was slightly sanded with 600-grit sand paper prior to each experiment to remove any possible contaminant. The 2^k factorial experiment with peak current and on-time as variables was conducted in random order with 2 replicates for each material.

Materials	Weight %
Aluminum 6061-T6:	96.7 Al, 0.6 Si, 1.0 Mg, 0.2 Cr, 0.15 Mn, 0.15 Ti, 0.27 Cu, 0.25 Zn, 0.7 Fe
Domex 550MC steel:	97.5 Fe, 1.80 Mn, 0.12 C, 0.1 Si, 0.15 Ti, 0.2 V
HSLA steel:	98.9 Fe, 0.80 Mn, 0.14 C, 0.1 Si, 0.005 Ti, 0.004 V
Brass CA 360:	61.5 Cu, 0.35 Fe, 3.0 Pb, 35.5 Zn

Table 1: Chemical compositions of tested materials (ASM; SSAB)

Properties	6061-T6	Domex 550MC	HSLA	CA 360
Density (g/cm^3)	2.7	8.13	7.81	8.49
Hardness (Brinell)	95	550	138	60
Melting temperature (°C)	582-652	1520	1527	1050
Shear strength (MPa)	207	371	260	235
Yield strength (MPa)	276	550	380	310
Tensile strength (MPa)	300	660	450	400
Specific heat (J/g/°C)	0.876	0.434	0.446	0.38
*Thermal conductivity (W/m°K)	177	41	52	110
*Thermal diffusivity (mm^2/s)	73	11.6	14.9	34
** Electrical resistivity (Ωm)	4.066×10^{-8}	17×10^{-8}	14.2×10^{-8}	6.6×10^{-8}

Table 2: Relevant physical and mechanical properties (ASM; SSAB; Ahmad, 2011)
*Estimated values from similar alloys (Kothandaraman and Subramanyan, 2013)
** Estimated values from similar alloys (www.nde-ed.org)

After die-sinking EDM operations, the outside diameters of drilled holes were measured with the Mitutoyo QS-E2010B vision system. A row of holes was then sectioned along the central plane on the Agies Charmilles Cut 20 wire EDM to reveal the hole profile and depth. Dimensions of sectioned profile and high resolution images were obtained with the Olympus STM6 measuring microscope with 0.1 µm resolution and an attached 12.1 Mpixel DP digital camera. Since the removal volume was not a perfect cylindrical shape, we calculated the volume in two steps:

i)   Calculating the removal area abcdefg (Figure 3b) by obtaining the total number of pixels and convert into area from the known area of a square and its pixels.

ii) Calculating the removal volume by rotating the area abcdefg about the hole symmetric axis. The 360° rotation action is done by sweeping a radius of D/4 one revolution.

$$V = A_r \frac{\pi D}{4} \tag{7}$$

And the MRR is calculated from:

$$MRR = \frac{V}{t} \tag{8}$$

Where
MMR: material removal rate
V: removed volume
t: EDM time

A_r: average removed area abcdefg (from left and right)
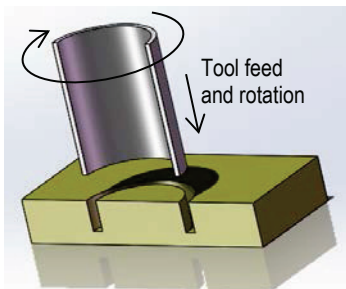D: outside hole diameter (from top view measurement)

Figure 2. Schematic of EDM using a rotating hollow electrode.
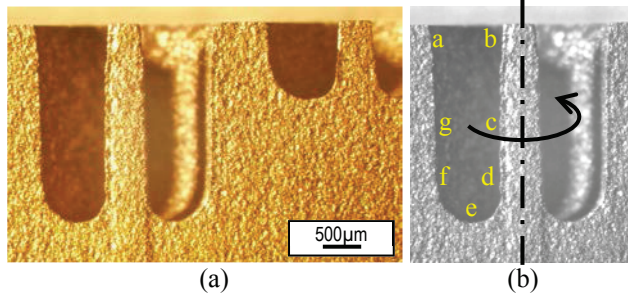

(a)   (b)

Figure 3. Centrally sectional view of EDM'ed brass holes at different EDM conditions. Notice the remaining of central pillar from a hollow electrode.

Data of the factorial experiments were entered and analyzed using Minitab software. Selected sectioned samples were cold mounted in epoxy, hand ground to 600-grit finish, then polished to 1-µm finish using alumina polishing compound. Ultrasonic cleaning of samples in isopropyl alcohol was done before and after grinding and polishing. The aluminum samples were etched in Keller etchant (190 ml water, 5 ml nitric acid, 3 ml hydrochloric acid, and 2 ml hydrofluoric acid) and the steel samples were etched in Nital etchant (5 ml nitric acid, and 100 ml ethanol) to reveal the microstructure below an EDM'ed surface.

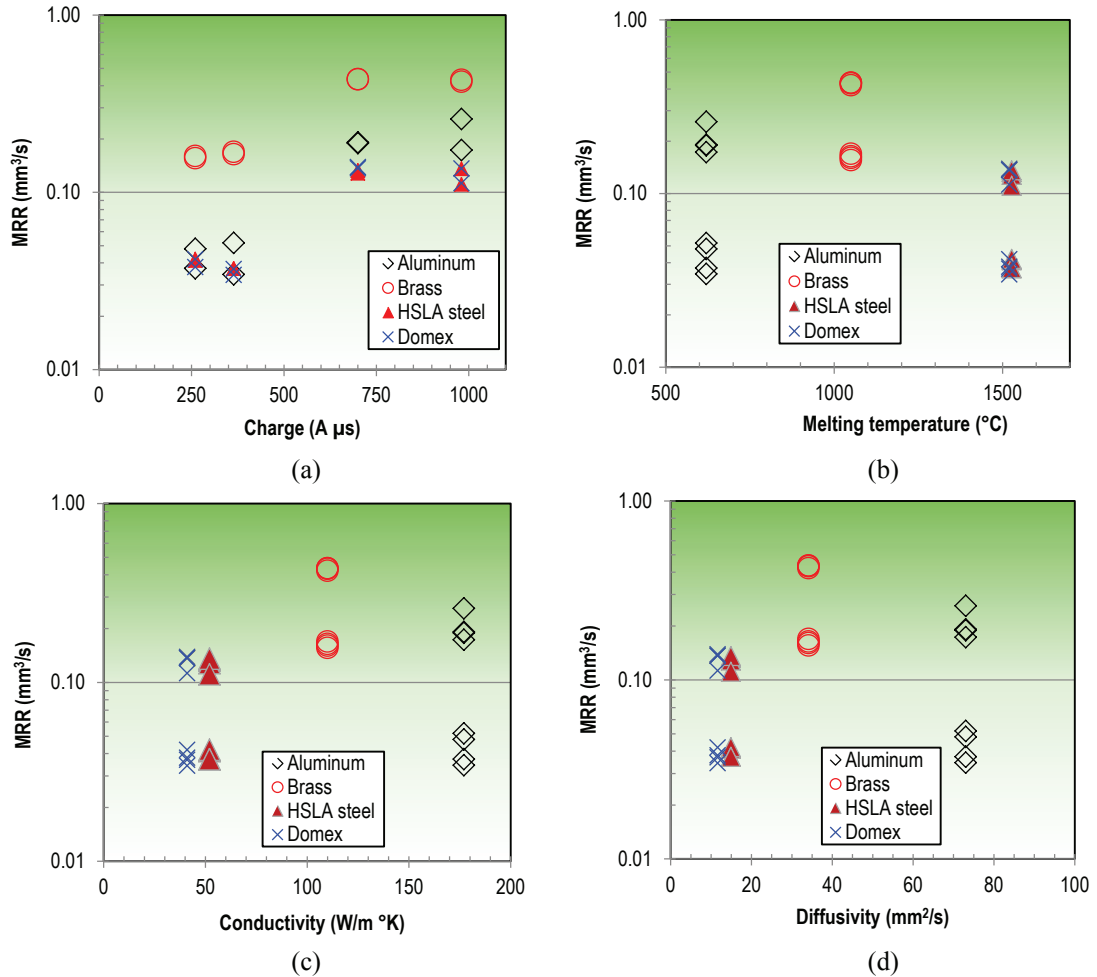# 4 Results and Discussions

Figure 4. Dependence of MRR on (a) electrical charge (I_p*t_{on}), (b) workpiece melting temperature, (c) workpiece conductivity, and (d) workpiece thermal diffusivity. EDM drilling at 13-35 A peak current, 20-28 µs on time, 50% duty cycle, 0.22 µF capacitance, 15-18s drilling time.

The dependence of MRR on peak current I_p, on-time t_{on} and material properties is sought. The dependence of MRR on both peak current and on-time has been reported as two separated variable as shown in equations (4-6). Since both current and on-time affect *MRR* as seen in the reviewed section, the product of I_p*t_{on} or cumulative charge of a sparking cycle is introduced. The dependence of MRR to the charge *Q* is shown in Figure 4a where log *MRR* and log *Q* is proportional. Increasing either or both I_p and t_{on} would improve MRR while compromising the EDM'ed surface finish (Bobbili et al., 2015; Goswami et al., 2014; Sultan et al., 2014). Data analyzing using Minitab utilizes the charge *Q* as a variable instead of peak current and on-time separately.

The dependence of *MRR* on workpiece material properties is not fully understood. The dependence of *MRR* on workpiece thermal properties includes melting temperature (Groover, 2010) and thermal diffusivity (Bobbili et al., 2015). Plots of *MRR* against thermal properties of workpiece materials are

shown for the effect of melting temperature (Figure 4b), thermal conductivity (Figure 4c) and thermal diffusivity (Figure 4d). Although brass has the highest MRR among other materials, its thermal properties are in between those from aluminum and steel (Table 2).

The following analysis assumes simple dependence of MRR on T_m as in equation (2). Using two variables $\log(Q)$ and $\log(T_m)$, the result of regression analysis of the factorial experiments on four materials in this study is summarized in Table 3.

Analysis of Variance

Source	DF	Adj SS	Adj MS	F-Value	P-Value
Regression	2	2.24354	1.12177	16.41	0.000
$\log(I_p*T_{on})$	1	2.03235	2.03235	29.73	0.000
$\log(T_m)$	1	0.21118	0.21118	3.09	0.089
Error	29	1.98238	0.06836		
Lack-of-Fit	13	1.93588	0.14891	51.24	0.000
Pure Error	16	0.04650	0.00291		
Total	31	4.22591			

Model summary

S	R^2	R^2 (adj)	R^2 (pred.)
0.261453	53.09%	49.85%	44.22%

Coefficients

Term	Coefficient	SE Coefficient	T-Value	P-Value	VIF
Constant	-2.34	1.08	-2.16	0.039	
$\log(I_p*T_{on})$	1.110	0.204	5.45	0.000	1.00
$\log(T_m)$	-0.537	0.305	-1.76	0.089	1.00

Table 3: Results of regression analysis.

From Table 3, the regression model to predict MRR is therefore:

$$MRR = \frac{Q^{1.11}}{10^{2.34}T_m^{0.537}} = \frac{\left(I_p . t_{on}\right)^{1.11}}{219\, T_m^{0.537}} \quad \text{with } t_{on} = t_{off} \tag{8}$$

The residual plots are shown in Figure 5. The relatively misfit of brass in the model is seen on Figure 5a when the MRR residual for brass is positive while it is negative for other materials. Since the experiments were conducted in random order, the residual does not form a pattern as seen in Figure 5b. Figures 5c and 5d show a good fit of the residual to a normal distribution curve. Referring to Table 3, the p-values for $\log(I_p*t_{on})$ and $\log(T_m)$ are practically zero and 0.089 respectively; this means the model can predict the dependence of *MRR* to the product of peak current and on-time with 95% confident level, but a lower confident level – perhaps 90% – is expected for predicting the effect of melting temperature on *MRR*.

Figure 6a and 6b shows the percentage error of MRR against the actual experimental data using equations (2) and (8). Significant deviation (1,000-8,000%) indicates that equation (2) cannot predict MRR precisely since it excludes the contribution of on-time. The error reduces to ±55% when using equation (8) when combining peak current and on-time as cumulative charges. Figure 7 summarizes the errors when using these two models; notice that the plot uses the absolute value of error for

displaying on the vertical log scale. Data from equation (8) are clustered about 50% error line while data from equation (2) are near the 5,000% error line which is two orders of magnitude higher.
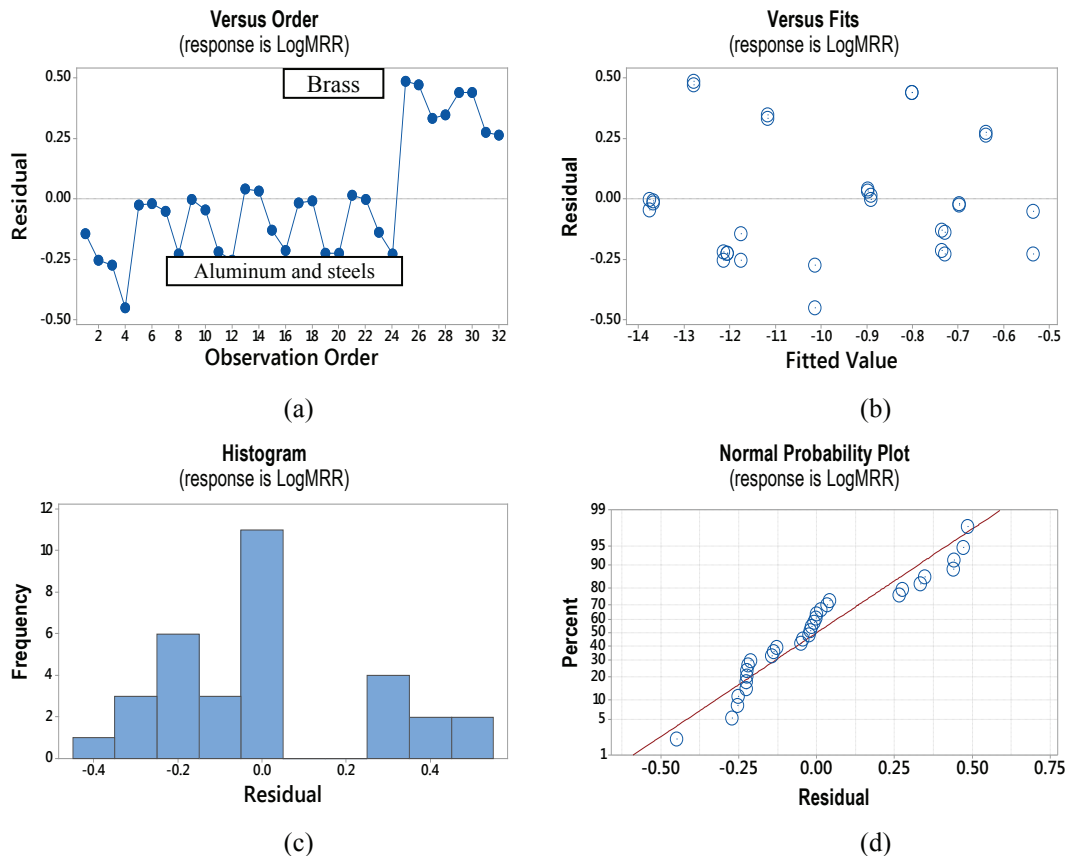

Figure 5. Residual plots for (a) log MRR, (b) fits, (c) histogram, and (d) normal distribution.

The low viscosity dielectric fluid is pumped through the center of a rotating cylindrical electrode at high pressure. The rotation of an electrode during EDM'ing would help to (i) improve a drilled hole roundness and its cylindricity, and (ii) improve debris flushing from bottom of a deep hole. Since the rotating speed is constant at 122 rpm for the Sodik K1C, there was no attempt to find quantitative relationship of electrode rotation speed on MRR and part quality.

Both MRR and surface quality are two opposite goals for users to choose from. When a workpiece material is removed at high MRR (i.e., high current and on-time), then the powerful sparks from discharging current heat, melt, and expel the materials to form small droplets of molten debris and leave a large crater behind. When flushing by dielectric fluid is inadequate – due to a short off-time or a low flushing pressure – then some molten debris would redeposit back onto the EDM'ed surface to form a recast layer. Such undesirable recast layer roughens the surface, contains possible defects such as microcracks, tensile residual stress, and porosity that are detrimental to the part reliability in service. Recast and defects are shown in Figure 8 for the Domex steel sample and in Figure 9 for the aluminum sample.

It is recommended that a two-pass EDM process should be practiced to achieve both high MRR and surface quality. The first roughing pass should use high charges (high current and long on-time) for high MRR; and the second finishing pass should use lower charges (low current, short on-time therefore EDM'ing at high sparking frequency) to remove the recast layer and possible defects while polishing the surface. A positive workpiece and negative electrode polarity also contribute to a better EDM'ed surface finish.

This initial study utilizes a two-level factorial experiment to identify and rank contributing variables that effect MRR and quality of a range of engineering materials after die-sinking EDM. Although equation (8) predicts the MRR better than equation (2), additional considerations will be considered in continuing research:

- A central composite design will be implemented to study possible non-linearity of MRR due to changing of process variables.
- Consistent electrodes should be used for each drilling experiment. A new electrode with square end would produce a different hole shape when comparing with hole drilling with a used electrode.
- Deep holes with aspect ratio 10:1 should be drilled. Such high aspect-ration drilling removes a large volume, minimizes error due to variation of electrode ends, and shows the effect of off-time on how effective the debris flushing would be.
- This study kept duty cycle constant at 50% for all experiments. A more aggressive EDM with higher duty cycle will be experimentally found without compromising the EDM'ed surface quality.
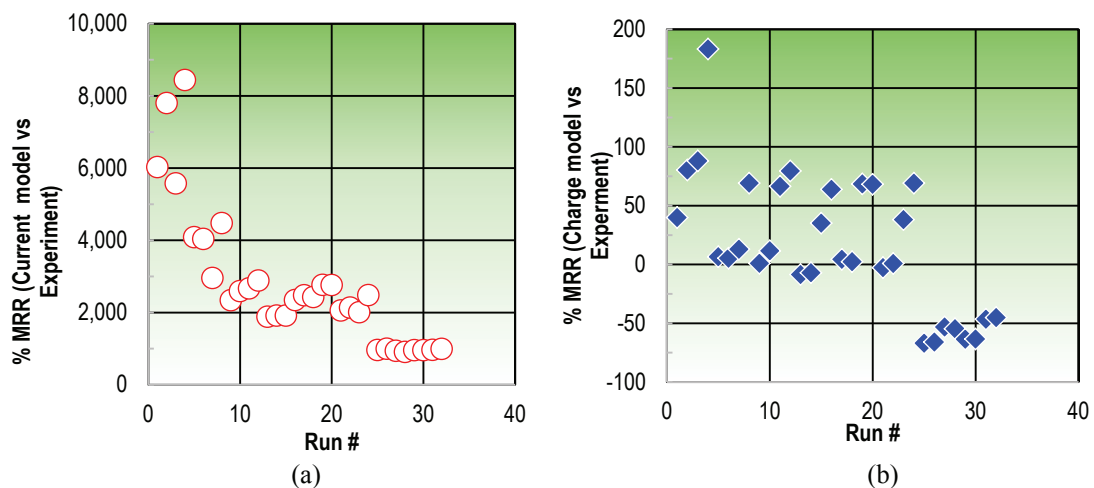

Figure 6. Prediction error for MRR models with parameters: (a) current and melting temperature, and (b) charge and melting temperature.
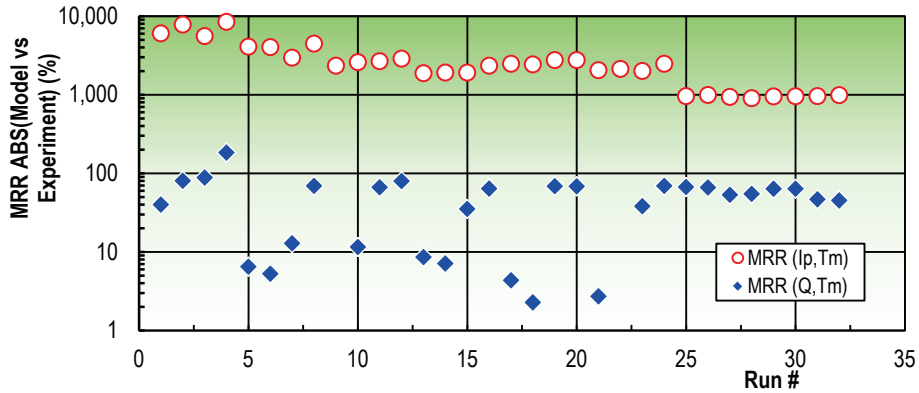
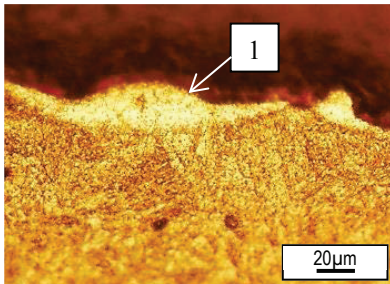**Figure 7**. Comparison of prediction error from two models.

Figure 8. Microstructure of Domex 550MC steel with recast layer (#1). EDM at 35A, 20µs on-time, Nital echant.
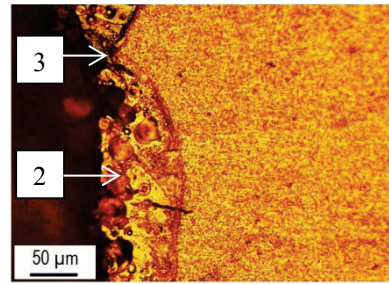

Figure 9. Microstructure of 6061-T6 aluminum with recast layer (#2) and thermal crack (#3). EDM at 53A, 30µs on-time. Keller etchant.

5 Conclusions and Recommendations

This study investigates the material removal rate (MRR) in die sinking electrical discharge machining (EDM). Hollow electrode for effective flushing was used on four different engineering alloys: aluminum, brass, high strength steel, and high strength low alloy steel. It was shown that:

1) The MRR depend on the cumulative electrical charges from each sparking cycle. The charge is calculated as the product of peak current and on-time for each cycle. Increasing the charge by setting a higher peak current and longer on-time would increase the MRR.

2) A regression model was proposed to predict the MRR. The model has a positive power term for cumulative charge per cycle, and a negative power term for melting temperature of a workpiece. The p-value for log(charge) is practically zero, but that for log(melting temperature) is 0.089. Despite of this, the proposed model can predict MRR of four materials to within ±55% error which is about two orders of magnitude closer to experimental data compared to that from a published model.

Future work would refine the model by considering thermal and electrical properties of the workpiece materials in additions to the process parameters. Deep hole drilling with central composite experimental design will be implemented to study the non-linearity of process variables for a wide variety of engineering materials.

References

Ahmad MS. Study of Dynamic Behaviour of Multi-Layered Structures Subjected to Blast Loading. Thesis, University of Cape Town, 2011.

American Society for Metals. http://asm.matweb.com [retrieved 1 May 2015].

Bobbili R, Mahhu V, and Gogia AK. Modelling and analysis of material removal rate and surface roughness in wire-cut EDM of armor materials. *Journal of Science and Technology* 2015; 664-668.

Collaboration for NDT Education. http://www.nde-ed.org [retrieved 10 Dec 2015]

Dave HK, Sesai KP, and Raval HK. Development of semi empirical model for predicting material removal rate during orbital electro discharge machining of Inconel 718. *Journal of Machining and Machinability of Materials* 2013; 13(2/3): 215-230.

Dave HK, Sesai KP, and Raval HK. Modeling and analysis of material removal rate during electro discharge machining of Inconel 718 under orbital tool movement. *Journal of Manufacturing System* 2012; 2(1): 12-20.

Goswami A and Kumar J. Investigation of surface integrity, material removal rate and wire wear ratio for WEDM of Nimonic 80A alloy using GRA and Taguchi method. *Journal of Engineering Science and Technology* 2014; 17: 173-184.

Guitrau EB, The Electrical Discharge Machining Handbook. Hanser Gardner publications, 1997. ISBN 9781569902424.

Kothandaraman C P and Subramanyan S, Heat and Mass Transfer Data Book, 8th ed., New Academic Science, 2013. ISBN 978-1781830048.

Miller SF, Shih AJ, and Qu J. Investigation of the spark cycle on material removal rate in wire electrical discharge machining of advanced materials. *Journal of Machine Tools & Manufacture* 2004; 44: 391-400.

Ojha K, Garg RK, and Singh KK. MRR improvement in sinking electrical discharge machining: A review. *Journal of Minerals & Materials Characterization & Engineering* 2010; 9(8): 709-739.

Shabgard M, Seyedzavvar M, and Oliaei SNB. Influence of input parameters on the characteristics of the EDM process. *Journal of Mechanical Engineering* 2011; 57: 689-696.

Singh H and Garg R. Effects of process parameters on material removal rate in WEDM. *Journal of Achievements in Materials and Manufacturing Engineering* 2009; 32(1): 70-74.

Singh H and Singh A. Effect of pulse on / pulse off time on machining of AISI D3 die steel using copper and brass electrode in EDM. *Journal of Engineering and Science* 2012; 1(9):19-22.

SSAB Incorporation. http://www.ssab.com/Global/DOMEX/Datasheets [retrieved 1 Mar. 2015].

Sultan T, Kumar A, and Gupta RD. Material removal rate, electrode wear rate, and surface roughness evaluation in die sinking EDM with hollow tool through response surface methodology. *Journal of Manufacturing Engineering* 2014; 259129: 1-16.

Weller EJ, editor. Nontraditional Machining Processes, 2nd edition. Dearborn, Mich: Society of Manufacturing Engineers, 1984. ISBN 9780872631335.

Yahya A, Andromeda T, Baharom A, Rahim AA, and Mahmud N. Material removal rate prediction of electrical discharge machining process using artificial neural network. *Journal of Mechanics Engineering and Automation* 2011; 1: 298-302.